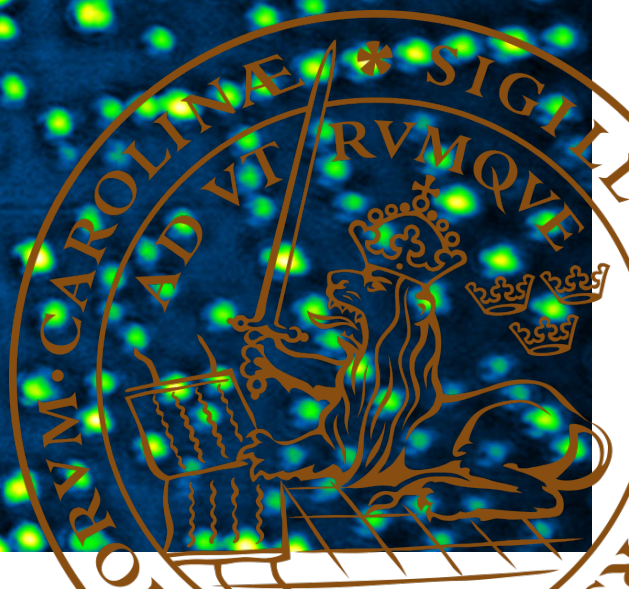




Polarisation-resolved super-resolution microscopy

WOUTER DUVERGER



Polarisation-resolved super-resolution microscopy

by

Wouter Duverger

This thesis is in partial fulfilment of the requirements for the degree of

MSc in Physics
Biological Physics and Computational Biology,

conducted at the
NanoLund Centre for Nanoscience, Lund University,
to be defended publicly on (**May 20, 2021**).

Project duration	4 months (full-time equivalent)
Supervision	prof. dr. Jonas Tegenfeldt
Daily supervision	dr. Jason Beech
Examiner	prof. dr. Edouard Berrocal



NANOLUND
NANOTECHNOLOGY FOR THE FUTURE

Abstract

Throughout this draft, I've marked todos for myself with (todo), and explicit questions to you with (question).

Table of Contents

Abstract	i
Table of Contents	ii
Nomenclature	iii
1 Introduction	1
2 Background	2
2.1 Diffraction-limited fluorescence microscopy	2
2.2 Super-resolution microscopy	4
2.3 Polarisation microscopy	5
3 Methods	9
3.1 Microscope setup	9
3.2 Conventional polarisation microscopy: acquisition and analysis	11
3.3 Polarisation-resolved STED microscopy (pSTED)	13
3.4 Samples	16
4 Results	17
4.1 Demonstration of conventional polarisation microscopy	17
4.2 Polarisation-resolved STED microscopy	17
5 Outlook	20
Bibliography	21
A Acknowledgements	24
B Code and data availability	25
C A note on laser safety	26
D Supplemental figures	28

Nomenclature

APD	Avalanche photodetector
AOM	Acousto-optical modulator
CCD	Charge-coupled device
FC	Filter cube
GFP	Green fluorescent protein
HWP	Half-wave plate
MPE	Maximum permissible exposure
NA	Numerical aperture
OD	Optical density (an OD2 filter reduces the light intensity by a factor of 10^2)
PBS	Polarising beam splitter
PMT	Photomultiplier tube
PSF	Point spread function
pSTED	Polarisation-resolved stimulated emission depletion microscopy
QWP	Quarter-wave plate
SiR	Silicon-rhodamine
SLM	Spatial light modulator
STED	Stimulated emission depletion microscopy
TCSPC	Time-correlated single photon counter

Introduction

- Molecular biology has had a great impact on our standards of living. There are a ton of diseases out there, and by studying how they work, we can (a) learn how cells and organisms function, and (b) propose certain treatments. Example: use amyloid aggregation to fight cancer.
- One interesting disease is caused by the *Yersinia* genus. *Yersinia pestis* is a species that caused the plague, which killed a third of the people living in europe and the plague of justinian. Vaccinations are available and incidence is low (600 cases per year worldwide), so low clinical importance currently.
- However, interesting mode of action. Actin filaments are broken down, revealing small self-organising micropatterns of actin left. Studying this might lead to new fundamental knowledge of cell function. (Ultimate goal of this research programme.)
- Current goal: set up a microscope system to study this disease, marrying super resolution microscopy and polarisation microscopy.

Microscopy - imaging structures at microscopic scales - is a wide and varied field. It is widely accepted to have began in the sixteen-hundreds, with Antoni van Leeuwenhoek's discovery of bacteria and other single-celled organisms [1]. After that, microscopes have been getting higher resolution, but as lenses got better and better, they were not the resolution bottleneck any more. Specifically, in 1873, Ernst Abbe determined that the best possible focus that a microscope can reach is limited by the wavelength of the light used [2]. This meant that the microscopes of the time were limited to a resolution of roughly 400 nm (assuming focused visible white light). It was long believed that the Abbe limit was a fundamental limit of nature, and that the only way around it was by using light of a different wavelength. This is one of the reasons for the development of electron microscopes [3], as quantum mechanics explains that accelerated electrons have much shorter wavelength than visible light.

Fluorescence microscopy is an invaluable tool in modern biology [4]. Unlike other methods, it is able to tag specific protein species and other relevant molecules in the cell with a fluorescent label. There are thousands of small organic fluorescent labels, and more are being developed [5, 6]. The introduction of GFP and other fluorescent proteins was a remarkable development in the field, as labels can now be genetically fused to proteins of interest [7, 8]. There were over thirty thousand papers collected in the PubMed database that mentioned fluorescence in the year 2020 alone.

- Super resolution (STED) was already set up and had polarisation capabilities, but were never used. My main contributions lie in figuring out what all components do, how to characterise them etc. Most of that will be found in the Background and Methods sections.
- Another big part of work was developing a new polarisation microscopy method (pSTED) to improve the angular resolution of a polarisation microscope. Relate pSTED to a figure in the *Yersinia* pattern paper.

2

Background

This section introduces concepts and techniques essential to this thesis. First, I will explain how fluorescence arises from discrete molecular energy states. Molecules can transition between these states by absorbing or emitting a photon with the right energy. Non-radiative transitions cause an energy difference between absorbed and emitted photons, which realises the potential of fluorescence microscopy. Then, I will explain how the wave nature of light limits the resolution of a microscope by limiting the size of the focal spot to roughly half the wavelength of the light used, and two methods to get around it. The first method, STED microscopy, uses targeted quenching of fluorescent molecules (also called dyes or fluorophores) at the outer edge of the focal spot to effectively narrow down the spot size. The second method exploits the polarisation state of excitation or emission light to measure the orientation of certain structures in a sample, even if their size is below the resolution limit.

2.1. Diffraction-limited fluorescence microscopy

In short, fluorescence is a phenomenon in which a molecule absorbs a photon of one wavelength, spends a short amount of time (a couple of nanoseconds) in an excited energy state, and then emits a photon of a wavelength longer than the first one. The difference in wavelength is essential to perform microscopy, and the fact that molecules have discrete energy states is key to get there.

Let us consider a molecule with two electronic energy states, each of which has a number of vibrational energy levels as in Figure 2.1. When the molecule is in its ground state (the lowest available energy level), it can absorb photons only if the energy they carry matches the difference between the ground state and another energy level. From an excited state, the system can relax into lower vibrational levels without emitting radiation, after which it emits a photon, relaxing back to the ground state. Two possible paths are shown in the figure. Because some energy is lost in a non-radiative way, the emitted photons will

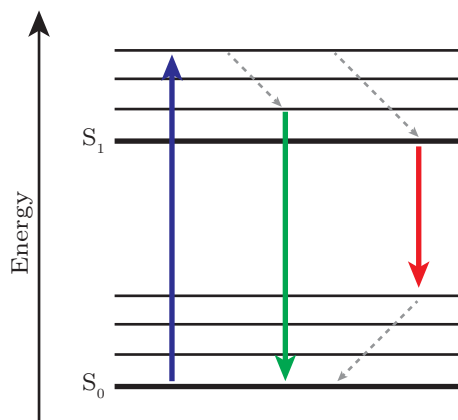
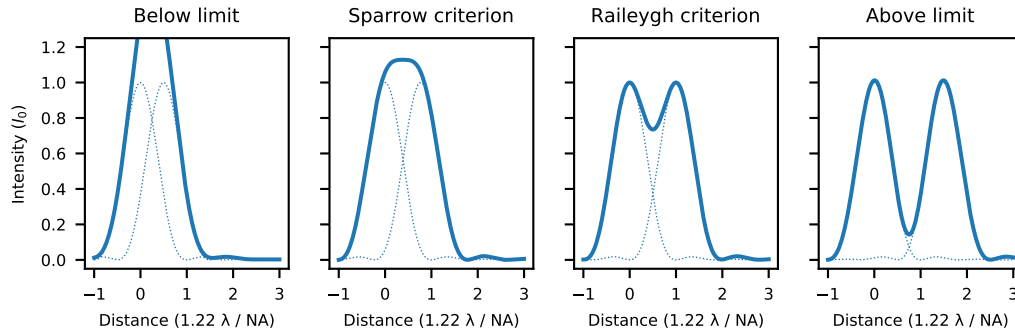


Figure 2.1: Illustration of the discrete energy states of a molecule and some possible transitions between them. The difference between energy levels determines the wavelength and colour of the absorbed or emitted photon.

Criterion	Definition
Rayleigh	The first minimum of one point's Airy function coincides with the maximum of another
FWHM	The width of the Airy function at half of the peak height
Abbe (what did he base it on?)	$d_{xy} = .5\lambda/\text{NA}$
Sparrow	The distance between fluorophores at which the central maximum splits
	$d_{xy} = .47\lambda/\text{NA}$

Table 2.1: Some common definitions of the resolution limit d_{xy} .**Figure 2.2:** Illustration of the diffraction limit. Below the resolution limit, two fluorophores (dashed) appear under a microscope as a single peak (solid, sum of the intensities of the two fluorophores).

carry less energy than the absorbed photon, resulting in the wavelength difference mentioned before. This is also called the Stokes shift.

The precise energy levels available depend on the molecule and its environment. Therefore, every fluorescent molecule has a unique absorption and emission spectrum, which needs to be considered when planning a fluorescence experiment.

We'll consider the diffraction limit in one of the simplest possible setups: an epifluorescence microscope. Epifluorescence microscopy is fairly similar to bright field microscopy; it is just using excitation light of a well-defined wavelength instead of white light. The sample, which is stained with a fluorescent dye, is illuminated at a wavelength that dye can absorb. The dye molecules will then emit photons of longer wavelengths in their emission spectrum, which are collected by the microscope objective. Before imaging by a CCD camera, the scattered laser light can be filtered away using a dichroic mirror that passes emission light and reflects excitation light.

It used to be the case that microscopes were limited in resolution by the quality of their lenses and the pixel density of the CCD, but there is a much more fundamental limit, first described by Ernst Abbe. This limit is caused by the presence of an aperture. When a beam of light goes through an aperture of finite size, such as a lens, it cannot be focused onto an infinitesimal point. Instead, it will generate a spot with a radius approximately equal to $\lambda/2\text{NA}$, where λ is the wavelength of the light and $\text{NA} = n \sin \theta$ is the numerical aperture, the product of the index of refraction and the sine of the half-cone angle of the acceptance cone.

In particular, a circular aperture will convert point sources in the sample plane to Airy patterns in the image plane. Mathematically, this can be described by a convolution product between the point spread function (PSF) h and the fluorophore distribution ρ ,

$$I(\mathbf{x}) = (h * \rho)(\mathbf{x}) := \int d\mathbf{x}' h(\mathbf{x} - \mathbf{x}') \rho(\mathbf{x}'), \quad (2.1)$$

where the triple integration over the three components of \mathbf{x}' is implied, resulting in an image I . When two fluorophores are close enough together that their PSFs overlap, they appear as a single object instead of two separate ones. This happens when the distance between them is around $\lambda/2\text{NA}$, and that is what determines the resolution of a microscope. The exact resolution depends on your definition of this minimum resolvable distance. There are several definitions, but they are all proportional to λ/NA . Some of them are listed in Table 2.1 and visualised in Figure 2.2.

For a long time, physicists thought this limit was practically unavoidable [9], but in the next sections, I will discuss two ways in which one can get information from a system below the resolution limit. The first

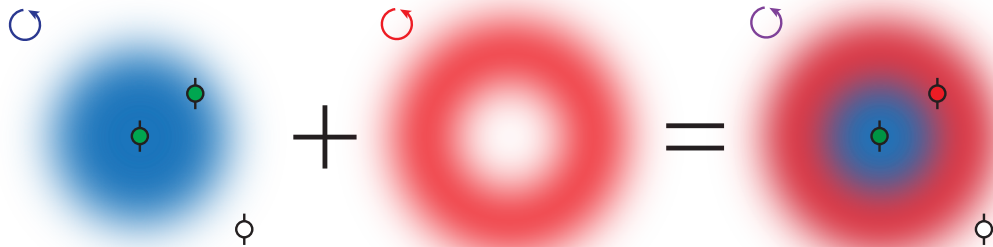


Figure 2.3: Working principle of STED microscopy. Fluorophores at the edge of the excitation PSF are quenched by stimulated emission, effectively resulting in a narrower PSF. Both beams are circularly polarised.

method (STED microscopy) directly increases the image resolution. The excitation light is still subject to the Abbe limit, but we add another laser to effectively improve our focusing. The first is indirect and requires playing with a new aspect of light (polarisation) that allows you to get orientational information about structures that are otherwise.

2.2. Super-resolution microscopy

There are several ways to increase image resolution, many of which use the photophysics of individual dyes to turn off a subset of them during imaging. Some methods do this stochastically, thereby increasing the average separation between fluorophores such that they are above the diffraction limit at all times. STORM (stochastic optical reconstruction microscopy) and PALM (photoactivated localisation microscopy) work this way [10, 11]. On the other hand, there are targeted techniques such as STED (stimulated emission depletion), GSD (ground state depletion), RESOLFT (Reversible saturable optical fluorescence transitions), and more [12–14]. The Tegenfeldt group own a STED microscope, so that is what I will focus on in this section.

In essence, a STED microscope is a confocal microscope with an extra laser that can selectively deplete fluorescence by stimulated emission. Its working principle is shown in Figures 2.3 and 2.4. In a confocal microscope, the excitation laser does not illuminate the whole sample at once, but is scanned over it. This means only fluorophores in an Airy disk around the focus will be excited. Furthermore, the detector is now comprised of a pinhole and a photodetector (not a camera), which filters out most of the out-of-focus light. Therefore, the PSF of a confocal microscope is the product of the laser PSF h_{exc} and the detection probability h_{det}

$$h_{conf}(\mathbf{x}) = h_{exc}(\mathbf{x}) \cdot h_{det}(\mathbf{x}). \quad (2.2)$$

(mention tradeoff between light collection (SNR) and z sectioning.)

Even though both of these PSFs are diffraction-limited, a STED microscope can reach an arbitrarily small resolution [15]. It does so by illuminating the sample with a donut-shaped laser at a wavelength longer than the emission wavelength. Referring back to Figure 2.1, the blue laser excites the fluorophores that emit in green, but a red transition is also allowed. Under illumination with a red laser, this transition is made more favourable by the process of stimulated emission, first postulated by Einstein in 1926 [16]. This way, fluorophores at the edge of the excitation PSF can be prevented from emitting green light, while fluorophores at the centre do not experience stimulated emission, which reduces the width of the effective point spread function. An illustration of this effect is given in Figure 2.3.

More rigorously, the STED beam depletes fluorescence according to

$$\eta(\mathbf{x}) = \exp(-\sigma_d h_d(\mathbf{x})), \quad (2.3)$$

which relates the fraction of fluorescence remaining as a function of the depletion intensity h_d . Therefore, the STED point spread function can be expressed as

$$h_{STED} = h_{exc}(\mathbf{x}) \cdot \eta(\mathbf{x}) \cdot h_{det}(\mathbf{x}), \quad (2.4)$$

which means the extent of the resolution improvement depends on the intensity of the depletion laser I_d . Harke et al. approximate the STED resolution to be

$$d_{STED} = \frac{d_c}{\sqrt{1 + d_c^2 a^2 \frac{I_d}{I_{sat}}}}, \quad (2.5)$$

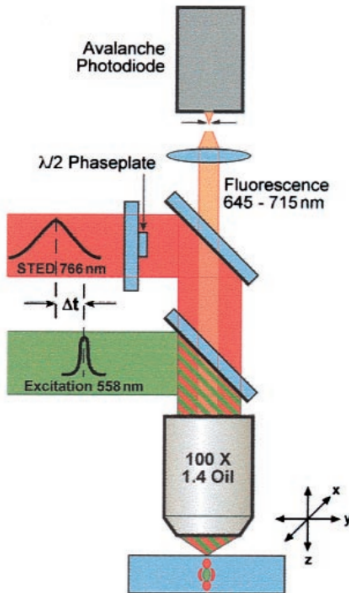


Figure 2.4: The rough layout of a STED microscope. The excitation laser is focused on the sample, and the STED laser forms a donut pattern around the focal spot. Emitted light is collected by the objective and focused on a pinhole before it is detected by an APD. Figure from Klar et al. 2000 [12]. ([Find a nicer figure or make your own.](#))

where d_c is the resolution limit of a confocal microscope, a the steepness of the donut pattern (i.e. high a means very tight central minimum in the donut-shaped intensity), and I_{sat} is the depletion intensity at which fluorophore brightness is reduced by half [17].

Although STED can reach an arbitrary resolution under optimal circumstances, the resolution reached in biological specimens is more usually around 50 nm [15, 18]. If information is desired at an even smaller scale using fluorescence microscopy, then other methods are required.

2.3. Polarisation microscopy

Polarisation microscopy uses the vectorial nature of light – the fact that light consist of EM waves that have a certain polarisation – to get orientational information of fluorophores below the resolution limit. Other methods to glean information below resolution include fluorescence resonance energy transfer (FRET) [19], for example, which is great for measuring distances between two fluorophores on the order of nanometres.

Among others, light polarisation microscopy has been used to measure how the structure of DNA changes when it is subject to a strong stretching force and how integrin proteins respond to an applied force and measure the order of molecules embedded in the cell membrane [20–23]. In this section, I will first introduce the concept of light polarisation, then discuss how it can be used in a microscope, and finally mention some optical components that affect the light polarisation, which are crucial to conducting a polarisation microscopy experiment.

For a more exhaustive introduction to polarisation microscopy, there are several good resources out there [24–26].

The polarisation ellipse. Light is a transverse electromagnetic wave. This means that there are oscillations of the electric and magnetic fields along the path of a light ray, and that these oscillations are orthogonal to the propagation direction. In other words, if the light propagates along \mathbf{k} , the electric and magnetic fields \mathbf{E} and \mathbf{B} must satisfy $\mathbf{E} \cdot \mathbf{k} = \mathbf{B} \cdot \mathbf{k} = 0$. (The fields themselves are also orthogonal to each other, so we can neglect \mathbf{B} without compromising our analysis.)

For the sake of simplicity, let's consider a ray propagating in the z direction. The electric field at any point in space and time can be written as

$$E_x(z, t) = E_{0x} \cos(kz - \omega t + \phi_x), \quad (2.6)$$

$$E_y(z, t) = E_{0y} \cos(kz - \omega t + \phi_y). \quad (2.7)$$

where \mathbf{E}_0 is the amplitude of the oscillation, k is the wavenumber (the length of \mathbf{k}), ω is the radial frequency and ϕ is an arbitrary phase. Note that the wavenumber and the frequency are related to each

Polarisation state	E_{0x}	E_{0y}	δ	Jones vector
Linear along x	1	0	any	(1, 0)
Linear along y	0	1	any	(0, 1)
Linear at $\pm 45^\circ$	1	± 1	0	(1, ± 1)
Circular (left-handed)	1	1	$\pi/4$	(1, i)
Circular (right-handed)	1	1	$-\pi/4$	(1, $-i$)

Table 2.2: List of a number of polarisation states (not normalised).

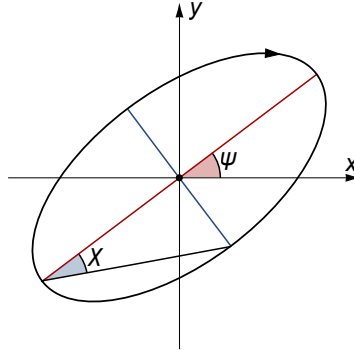


Figure 2.5: The meaning of ψ and χ in the context of the polarisation ellipse. [Figure by Wikipedia user Inductiveload]

other through the speed of light c , since $\omega = kc$. Note also that the x and y components can have a phase difference.

Letting $\delta = \phi_y - \phi_x$, it can be shown that

$$\left(\frac{E_x}{E_{0x}}\right)^2 - 2 \cos \delta \frac{E_x}{E_{0x}} \frac{E_y}{E_{0y}} + \left(\frac{E_y}{E_{0y}}\right)^2 = \sin^2 \delta. \quad (2.8)$$

This is the equation for an ellipse. That means that, at any point in time, the point (E_x, E_y) lies on the ellipse defined by the equation above, which is called the polarisation ellipse, which is completely determined by E_{0x} , E_{0y} and δ . Together, these values determine whether the polarisation is linear, circular, or something in between. Refer to Table 2.2 for an overview.

In general, the polarisation ellipse can be defined by means of two angles: the orientation ψ and ellipticity χ , as shown in Figure 2.5. They can be calculated from $\alpha = \arctan(E_{0y}/E_{0x})$ and the phase difference δ using

$$\tan 2\psi = \tan 2\alpha \cos \delta, \quad (2.9)$$

$$\sin 2\chi = \sin 2\alpha \sin \delta. \quad (2.10)$$

These are useful concepts because they are relatively easy to calculate from intensity measurements. Therefore, I will use these when I characterise laser beams in the setup.

Microscopy. Why is this relevant to microscopy? Well, the probability of excitation is dependent on the polarisation of incoming light. Since a fluorophore can be considered a small dipole moment, it will not interact with radiation that is orthogonal to the fluorophore. If the excitation laser is polarised along an angle ψ and the dipole is oriented along θ , the intensity of light emitted by that fluorophore will satisfy

$$I(\psi, \theta) \propto \cos^2(\psi - \theta). \quad (2.11)$$

This is Malus's law. Analogously, light emitted from a fluorophore is always linearly polarised parallel to its dipole. One can place a linearly polarising filter in front of the detector to measure a fluorophore's orientation. If the polariser emits light polarised at an angle ψ , then the intensity measured at the detector also follows Malus's law, meaning that these two setups are analogous (not taking into account depolarisation effects in an experimental setup). As an example, see Figure 4.1. Dipole excitation by circularly polarised light is not dependent on θ .

Common polarisation microscopy protocols include: rotating a linearly polarised excitation laser, rotating a polarising filter in the excitation beam path, or doing both. The first polarisation measurements

were done by excitation the sample with a linearly polarised laser and measuring the fractions of emission intensity that were parallel and orthogonal to the excitation light. As a result, one can calculate the anisotropy of a sample [27].

Jones calculus. Lasers are usually linearly polarised, but I have not yet mentioned how we can manipulate this polarisation to run the experiments we want. There are optical elements such as waveplates that can do this for us, and the best way to understand them is through Jones calculus. This is an incredibly useful way to model light polarisation, but it does require us to express the electric field with a complex function. Let us express it as follows:

$$\mathbf{E}(z, t) = \mathbf{E}_0 e^{i(kz - \omega t)}. \quad (2.12)$$

In the following analysis, we will treat \mathbf{E} as a two-dimensional vector with only an x and y component, as $E_z = 0$. Note that complex numbers are just a mathematical trick. The Maxwell equations that govern light propagation are linear, and taking the real part of a complex-valued function is also a linear operation, so the complex extension of \mathbf{E} will behave exactly the same as the actual electric field would. The phase difference between the two components is now contained in \mathbf{E}_0 , which can be expressed as

$$\mathbf{E}_0 = \begin{pmatrix} E_{0x} \\ E_{0y} e^{i\delta} \end{pmatrix}. \quad (2.13)$$

The Jones vectors for some special polarisation states are listed in Table 2.2.

The usefulness of Jones calculus lies in its ability to represent optical components as matrices acting on this vector. For example, a polariser that transmits x -polarised light has the following matrix form:

$$S_p = \begin{pmatrix} 1 & 0 \\ 0 & 0 \end{pmatrix}. \quad (2.14)$$

It is easy to verify that $S_p \mathbf{E}_0 = E_{0x}$. We also need to take into account how mirrors affect polarisation. A mirror flips the field component that is orthogonal (the s -component) to the mirror surface, while keeping the other component (p) unchanged. So, a mirror whose surface is parallel to the x -axis has a Jones matrix of the form

$$S_{mx} = \begin{pmatrix} 1 & 0 \\ 0 & -1 \end{pmatrix}. \quad (2.15)$$

Another important type of optical component in our setup is a waveplate. Waveplates or phase retarders are birefringent crystals (such as quartz), meaning the index of refraction a ray of light experiences is dependent on its polarisation. This happens when a crystal structure lacks cubic symmetry. When the coordinate system is aligned with the crystal axes, we might find that $k_x = k_z = k_o$ (the ordinary axes), while $k_y = k_e$ (the extraordinary axis). In these crystals, Equation 2.12 is no longer valid and should be substituted by

$$\mathbf{E}(z, t) = \begin{pmatrix} E_{0x} e^{i(k_o z - \omega t)} \\ E_{0y} e^{i(k_e z - \omega t + \delta)} \end{pmatrix}. \quad (2.16)$$

This can also be written in the form

$$\mathbf{E}(z, t) = \begin{pmatrix} E_{0x} \\ E_{0y} e^{i(\Gamma(z) + \delta)} \end{pmatrix} e^{i(k_o z - \omega t)}, \text{ where } \Gamma(z) = (k_e - k_o)z. \quad (2.17)$$

As one can see, a waveplate only imparts a delay on the y -component of a beam, depending on its thickness z and its birefringence. We can neglect phase factor common to both components and represent the action of a waveplate by the following Jones matrix,

$$S_\Gamma = \begin{pmatrix} 1 & 0 \\ 0 & e^{i\Gamma} \end{pmatrix}. \quad (2.18)$$

Generally, waveplates are characterised by the relative delay they impart on the slowly propagating polarisation component. Quarter-wave plates delay it by a quarter of a wavelength compared to the fast propagating ray, corresponding to $\Gamma = \pi/2 + 2n\pi$ (for any integer n). Therefore, the Jones matrix of a quarter-wave plate satisfies

$$S_{\lambda/4} = \begin{pmatrix} 1 & 0 \\ 0 & i \end{pmatrix}. \quad (2.19)$$

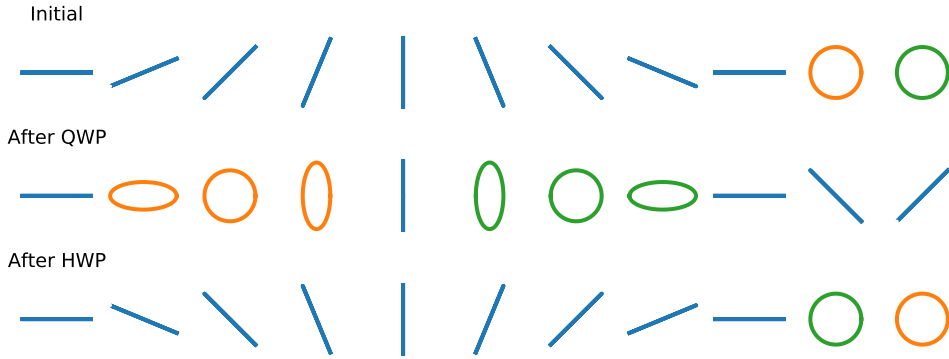


Figure 2.6: The effect of quarter-wave plates (QWP) and half-wave plates (HWP) on the polarisation ellipse. Orange: left-handed polarisation. Green: right-handed polarisation.

Let's consider what happens to some specific cases. If vertically or horizontally polarised light passes through a quarter-wave plate, its polarisation will not change. But light polarised along $+45^\circ$ (-45°) will be turned into left-handed (right-handed) light, and vice versa. Therefore, a quarter-wave plate allows us to convert between linearly and circularly polarised light, as shown in Figure 2.6.

The second type of waveplate we should treat is a half-wave plate. It features a delay of $\Gamma = \pi + 2n\pi$, and its Jones matrix looks like

$$S_{\lambda/2} = \begin{pmatrix} 1 & 0 \\ 0 & -1 \end{pmatrix}, \quad (2.20)$$

which corresponds to mirroring the polarisation state along the x -axis. Another way to think about that is that a ray polarised along an angle ψ will be rotated by an angle -2ψ . Circularly polarised light will get the opposite handedness, see Figure 2.6.

As said before, the power of Jones calculus lies in its ability to model the behaviour of a sequence of optical elements at arbitrary rotations. First, we need to define the Jones matrix for a rotated component. This is simply

$$S(\theta) = R(\theta) \cdot S \cdot R(-\theta) \quad , \text{ where } R(\theta) = \begin{pmatrix} \cos \theta & -\sin \theta \\ \sin \theta & \cos \theta \end{pmatrix} \quad (2.21)$$

and θ is the angle of the component's x -axis with the lab coordinate system's x -axis. As an example, we can send x polarised light through a polarising filter at an angle θ , which gives us

$$I(\theta) \propto \left| S_p(\theta) \cdot \begin{pmatrix} 1 \\ 0 \end{pmatrix} \right|^2 = \cos^2 \theta. \quad (2.22)$$

That is Malus's law, as we had defined before. We can also recover the same behaviour by using a fixed polarised and a half-wave plate at an angle $\theta/2$

$$I(\theta) \propto \left| S_p(0) \cdot S_{\lambda/2}(\theta/2) \cdot \begin{pmatrix} 1 \\ 0 \end{pmatrix} \right|^2 = \cos^2 \theta. \quad (2.23)$$

Jones calculus also has its limitations, the main one being that it cannot represent unpolarised light (an incoherent sum of different polarisations). Müller calculus, based on real-valued 4D Stokes vectors instead of the complex 2D Jones vectors, can handle it. As such, Müller calculus can also quantify depolarisation induced by non-ideal microscope optics. In this thesis, I mainly used Jones calculus to develop a theoretical understanding of the optical elements in the STED microscope, so using Müller matrices was not necessary. In the next sections, I will use the theory presented here to implement polarisation microscopy on the Tegenfeldt STED microscope. I will even develop the theory further to extend the concept of the optical point spread function into polarisation space.

3

Methods

(intro?)

3.1. Microscope setup

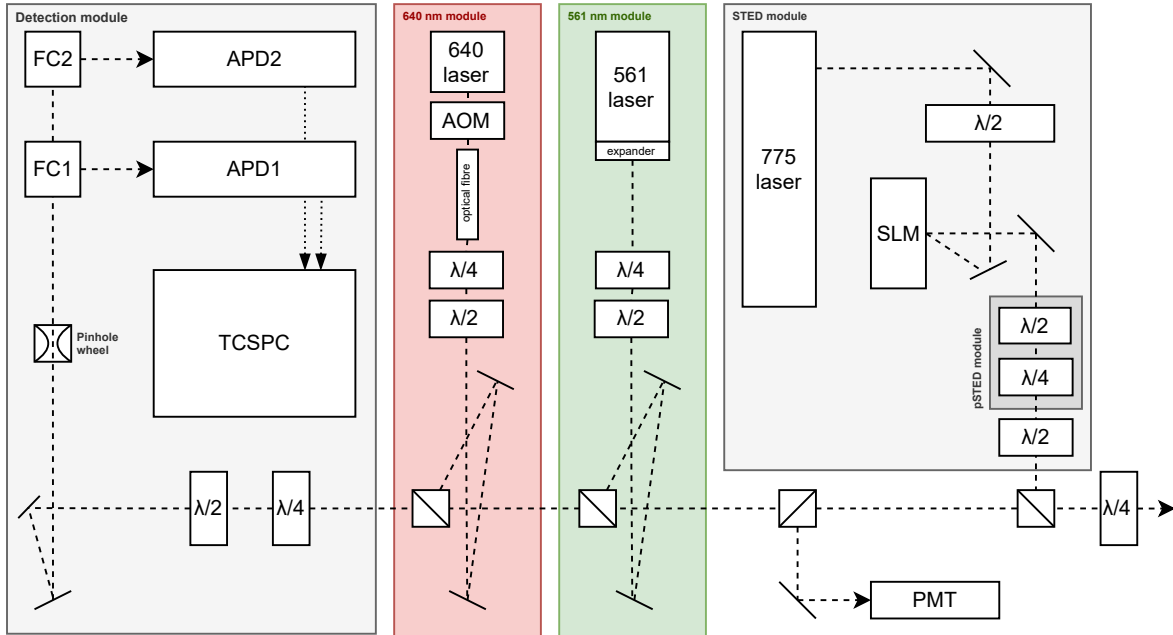


Figure 3.1: Schematic overview of the Tegenfeldt microscope. The sample is located in a microscope housing on the bottom right (outside this figure). FC1 and FC2 are swappable filter cubes. Half-wave and quarter-wave plates are denoted $\lambda/2$ and $\lambda/4$, respectively. Dashed lines represent the light path, except those that go to the TCSPC (those are digital connections). The waveplates in the pSTED module were not in the original setup, and were added as part of this project. See text for more details.

In short, the Tegenfeldt microscope is a confocal fluorescence microscope constructed by Abberior Instruments GmbH (Germany). It features two excitation lasers (at 561 nm and 640 nm) and one depletion laser at 775 nm for two-channel confocal or STED microscopy. It also contains a time-correlated single photon counter (TCSPC) for fluorescence lifetime imaging microscopy (FLIM) and a highly sensitive photomultiplier tube (PMT). Refer to Figure 3.1 for the layout of these optical elements. Samples are located inside an inverted Nikon microscope body (Ti-E, not shown in the figure) equipped with a piezo stage (M-687 PILine XY-stage system and P-736 PInano (Physik Instrumente) Z Microscope Scanner), a 60x, 1.4 NA oil immersion objective (Nikon Plan Apo) and a QUADScan beam scanner (Cambridge Technology).

In this section, I will address all laser lines as well as the detection module in detail, with a focus on characterising the light polarisation at different points in the microscope.

Table 3.1: Polarisation characteristics of the lasers. Shown are linearity I_{max}/I_{min} , ellipticity χ_E (χ_I) of the electric field (intensity), and ellipse orientation ψ . This data is based on Figure D.2.
 ((1) I display both $\chi_I = \arctan(I_{max}/I_{min})$ and $\chi_I = \arctan(E_{max}/E_{min})$. χ_I is the easier one to calculate but χ_E is the more established definition. What do you think I should go with? Maybe just both? (2) Can I list the quality of the pSTED polarisation here? It's very premature, but a nice place to get an overview of all lasers.)

Laser source	I_{max}/I_{min}	χ_I (deg)	χ_E (deg)	ψ (deg)
561 nm, linear	23.6	2.42	11.6	0
561 nm, circular	1.14	41.2	43.1	20
640 nm, linear	6.13	9.25	22.0	0
640 nm, circular	1.59	32.2	38.5	120
775 nm, circular	1.61	31.8	39.2	40

The laser modules. The fast-switching 561 nm laser is initially horizontally polarised, but the polarisation can be tuned by three waveplates in its path. The last one, a quarter-wave plate, is fixed in its rotation angle. In the standard mode of operation, excitation laser light should be circularly polarised to minimise resolution reduction due to lens distortion etc. [17]. In that mode, the (fast or slow) axis of the first quarter-wave plate should be aligned with the laser, such that it does not affect polarisation and the half-wave plate should be set such that it rotates the (linearly polarised) light to 45° with respect to the second quarter-wave plate. See Table 3.1 for the polarisation characteristics in the calibration provided by Abberior. The 561 nm laser is quite well-calibrated. In circular polarisation, it reaches a χ very close to perfectly circular (45°).

The 640 nm laser does not have fast-switching built in, so instead the light is fed into the microscope through a polarisation-polarisation optical fibre by an acousto-optical modulator (AOM). The AOM is a crystal in the beam path, in which sound waves can be generated by a piezo element. The ray is deflected by an angle that depends on the frequency of these waves, such that the laser beam can quickly be aligned into or away from the fibre aperture. The rest of the beam path is very similar to the 561 module, but the calibration of the waveplates in this pathway are not as accurate. Refer to Table 3.1.

The depletion laser travels through an entirely different set of optics than the excitation lasers to generate a donut beam. First, it travels through a half-wave plate that aligns the polarisation to the SLM (spatial light modulator). This HWP is necessary because an SLM adds an arbitrary spatially patterned phase delay to incident light, but only to the component polarised along its active axis. It will not alter the phase of the orthogonally polarised component. Using the proper phase delay patterns, one can create any (diffraction-limited) image in the sample plane. In our case, that would be a donut shape. Then – and I am ignoring the pSTED module for now, since that was not included in the original setup – the beam travels through a half-wave plate to ensure circular polarisation in the sample plane (after going through a quarter-wave plate at 45° to the QWP axes), just like the excitation lasers. This is done to ensure that the depletion efficiency does not depend on sample orientation and to avoid polarisation-dependent PSF distortion by lenses and other optics. The quality of the STED polarisation is similar to that of the 640 nm laser. Note that this is actually a significant result, as that means the donut beam is not isotropically polarised. It will be far more effective at quenching fluorophores oriented at 40° than those at 130°.

One more thing we can derive from this data (see Figure D.2), is that the 640 laser needs to ramp up every time it is powered on, due to the lack of fast switching. This can be somewhat prevented by setting the laser “always on”, albeit at a power of 0%. Furthermore, at low powers, the laser intensity may not be proportional to the the power setting in software. Their actual relationship is shown in Figure D.1. If experiments need to be done at low power, a neutral density filter is required. This is luckily not the case for biological specimens with a low density of fluorophores.

Looking at the calibrations of the waveplates in the excitation modules (Figure D.3), one can see that they move quite erratically, but they do work, as shown in Figure D.2. This could be an effect of the automated calibration performed by Abberior. In the 561 nm calibration, for example, one can see that the QWP constantly flips between about 30° and 120°, which are 90° apart. (I should look at these in more detail!)

Finally, I also measured the PSFs of the lasers, by scanning over a reflective gold bead and acquiring an image on the PMT. These are shown in Figure D.4.

The detection module. The main detectors of the microscope are a set of avalanche photodiodes (APDs), but there is also a highly sensitive photomultiplier tube (PMT) right after the QWP on the

microscope end. The PMT is usually used to measure the point spread functions of the lasers and to align them. In normal operation, the light travels on to the detection waveplates, then through a pinhole wheel, passes filters and dichroics in the filter cube housings, and is finally reflected onto the APDs. The wheel contains pinholes of different sizes, which allows for choosing the trade-off between light collection and z resolution. Different filter cubes are available with various bandpass filters, dichroic mirrors, and/or a polarising beam splitter (PBS).

The APDs show a slight polarisation sensitivity, of about 10% of the maximum sensitivity (see Figure D.5). I measured this by exciting Tetraspec beads with the 561 laser set to circular excitation, such that the emission light is non-polarised. Then I placed a linear polariser behind the detection waveplates and measured their signal as a function of polariser angle. It seemed like the beam moved depending on the incident polarisation, as aligning the APDs when the signal was minimal did help a little, but the imperfect circularity of the 561 laser may also play a role, as it is on the same order of magnitude. ([Try to correct APD sensitivity data with 561 laser polarisation?](#))

We did have some problems with the waveplates in the detection module. They can be controlled through Abberior's software suite (Imspector), but it is not clear if they are set up correctly. The calibration is based on a control angle that I will call θ . It would theoretically be possible for this setup to rotate polarised light of any orientation, since

$$S_{\lambda/2}(\theta/2)S_{\lambda/4}(0)S_{\lambda/4}(0) = \begin{pmatrix} \cos \theta & -\sin \theta \\ \sin \theta & \cos \theta \end{pmatrix}, \quad (3.1)$$

which is simply the rotation matrix $R(\theta)$. The exact position of the quarter-wave plates does not matter, but it is important that they are aligned with each other. If the waveplates are at a different angle ϕ , then this set of waveplates rotates the polarisation by an angle $(\theta - 2\phi)$ instead. I developed a new calibration, since we did not understand the goal of the original one. If we approximate the default calibration with a QWP at θ and a HWP at 0, then the action of these waveplates would be

$$S_{\lambda/2}(0) \cdot S_{\lambda/4}(\theta) \cdot S_{\lambda/4}(0) = \begin{pmatrix} \cos^2 \theta + i \sin^2 \theta & (1+i) \cos \theta \sin \theta \\ (-1+i) \cos \theta \sin \theta & \cos^2 \theta - i \sin^2 \theta \end{pmatrix}. \quad (3.2)$$

It is unclear what goal that would serve. To develop my own calibration, I first had to figure out what angle to set the second quarter-wave plate to in order to align it to the first one. I did this by placing a polariser in the sample holder (P1) and illuminating it with the top lamp, such that the light incident on the first quarter-wave plate was linearly polarised. Then I placed another polariser (P2) after the waveplates that I rotated to assess the linearity of the polarisation there. Aligning the quarter-wave plates with each other simply involved maximising the linearity of the light after the waveplates.

Second, I assessed both Abberior's and my calibration. As presented in Figure 3.2, my calibration works really well. However, changing P1 seems to mess up that idea. The detection waveplates seem to rotate the polarisation for P1 at 0° or 90° , but seem to circularise incoming light at 45° and 135° to a certain extent, such that the polarisation rotation is less effective. This needs to be fixed before we can confidently use polarisation-affecting elements in the detection path.

Third, I checked the POL cube, which seems to work as expected. ([Put figure in appendix.](#))

3.2. Conventional polarisation microscopy: acquisition and analysis

Because the current setup offers so much control over the light polarisation on both the excitation and detection ends, one can perform polarisation microscopy in several different ways:

1. Measuring the intensity of emission components parallel and orthogonal to linearly polarised excitation (I_{\parallel} and I_{\perp}). This is a very established method of polarisation microscopy, and allows for making anisotropy images, where every pixel is calculated according to

$$r = \frac{I_{\parallel} - I_{\perp}}{I_{\parallel} + 2I_{\perp}}. \quad (3.3)$$

2. Detection of emission polarised at different angles after circular polarisation.
3. Detection of total emission intensity as a function of the polarisation angle of excitation light.

Methods 1 and 2 require the PBS cube to be placed in one of the FC housings. When placed in FC1, the PBS cube reflects s -polarised light (vertical) into APD1 and transmits p -polarised light (horizontal) to be collected by APD2. Unfortunately, we cannot use these methods yet, since they rely on the action of

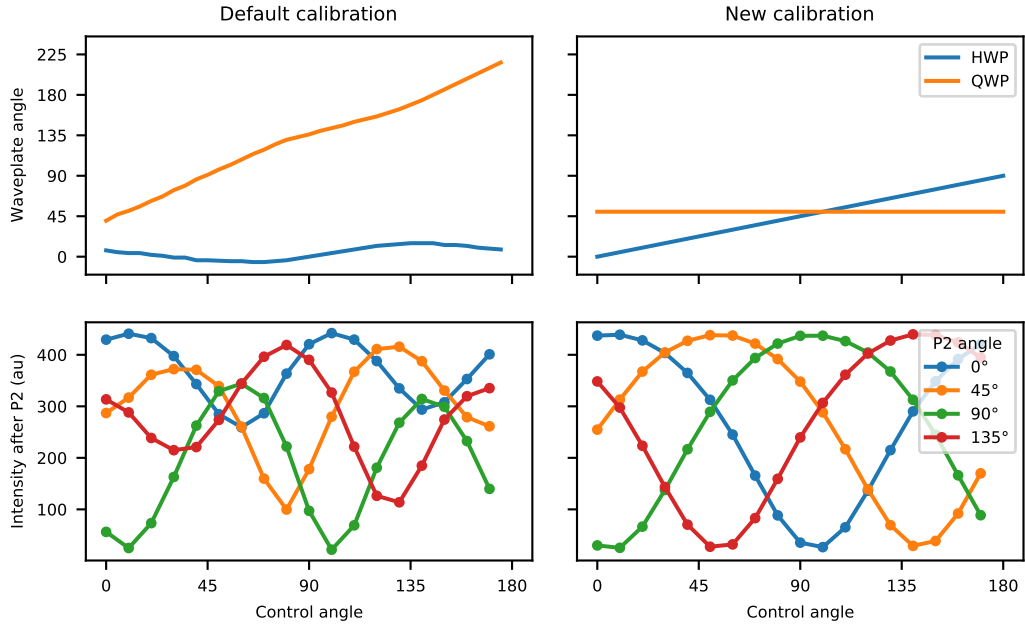


Figure 3.2: A comparison of the default detection waveplate calibration and the new one. The new calibration seems to actually rotate incident polarisation by an arbitrary angle.

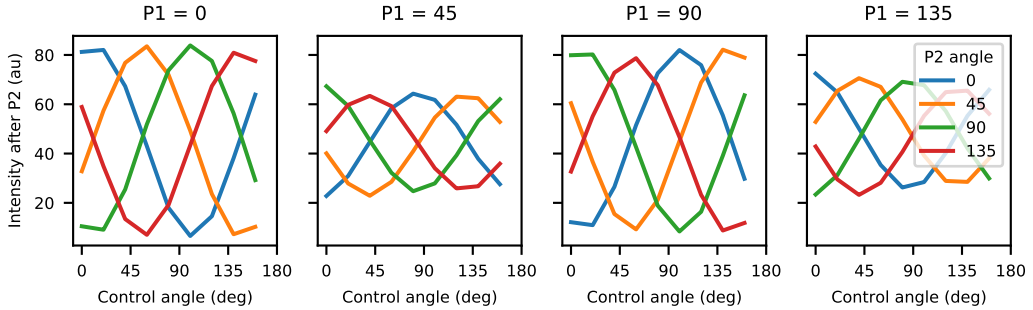


Figure 3.3: The effect of rotating the incoming polarisation (P_1). The detection waveplates seem to rotate the polarisation for P_1 at 0° or 90° , but seem to circularise incoming light at 45° and 135° somewhat.

the detection waveplates, even if they are not actively used during the acquisition. Once we do, however, the waveplates can be used to sample more than two angles during an acquisition. This is necessary to distinguish between light polarised along $\pm 45^\circ$, since these two angles give exactly the same intensity when sampling at 0° and 90° degrees.

The last method, however, is not subject to those constraints, and is already achievable on the Tegenfeldt microscope. I have carried out some acquisitions and wrote some code for analysing this data. The process of acquiring and analysing these images goes as follows:

1. Acquire a stack of images at different excitation polarisation angles θ_n . Then we have a three-dimensional array of intensity values I_{nxy} .
2. Align images in this stack with each other, as the excitation beam seems to move as a function of polarisation angle. The alignment algorithm will be explained later.
3. Compensate for photobleaching.
4. For every pixel, calculate the Fourier coefficient corresponding to a 180° -periodic signal.
5. Based on that information, construct a new image in the HSV (hue, saturation, value) colour space where pixel colour depends on the polarisation direction, the saturation shows the degree of polarisation and the brightness (value) shows the total intensity of a pixel.

Stack alignment. Images in a stack are aligned using an ECC optimisation algorithm partly implemented in the OpenCV library [28]. The goal is to generate a new stack I'_{nxy} corrected for sample or

beam drift. We will take the first frame as reference, setting

$$I'_{0xy} = I_{0xy}. \quad (3.4)$$

For every other frame I_{nxy} , we can calculate a warp matrix using the `findTransformECC()` method defined in OpenCV that maximises the correlation between I_{nxy} and $I'_{(n-1)xy}$. We only calculate translational motion, so scaling and rotation are not allowed. Finally, we transform the original image using that warp matrix and `warpAffine()` and save the result as I'_{nxy} , in other words:

$$I'_{nxy} = \text{warpAffine}\left(I_{nxy}, \text{findTransformECC}\left(I'_{(n-1)xy}, I_{nxy}\right)\right) \quad \text{for all } n > 0. \quad (3.5)$$

Bleaching compensation. Since we want to calculate Fourier coefficient, we need to separate the photobleaching response from the polarisation response. We can do this by comparing two frames at identical polarisations and estimate the bleaching rate by their difference. Unfortunately, the Imspector software suite does not allow for rotating the excitation polarisation by more than 175° , so we cannot do this exactly. We would be able to if we also used a PBS, but that is not an option, as explained before. Let \bar{I}_0 be the mean intensity of the first image, and \bar{I}_N the mean intensity of the last one. For now, we simply estimate the bleaching per frame as

$$r = \sqrt[N]{\frac{\bar{I}_N}{\bar{I}_0}}, \quad (3.6)$$

given $N+1$ number of frames were acquired. Then we can compensate for photobleaching by multiplying every frame with a correction factor as

$$I''_{nxy} = r^{-n} I'_{nxy}. \quad (3.7)$$

This is far from perfect, but good enough for now.

Colouring the image. For every pixel, calculate a complex-valued Fourier coefficient corresponding to a period of 180° (at which we should see polarisation dependence) using

$$F_{xy} = \sum_n I''_{nxy} e^{i2\theta_n}. \quad (3.8)$$

Then construct an image in the HSV (hue - orientation, saturation - degree of polarisation, value - total intensity) where

$$h_{xy} = \arg(F_{xy}), \quad (3.9)$$

$$s_{xy} = |F_{xy}| / v_{xy}, \quad (3.10)$$

$$v_{xy} = \sum_n I_{nxy}. \quad (3.11)$$

Finally, normalise these channels c to be in the range $(0, 1)$ and optionally apply a power law with a manually chosen coefficient α_c for optimal visualisation,

$$c'_{xy} = \left(\frac{c_{xy}}{\max(c_{xy})} \right)^{\alpha_c}. \quad (3.12)$$

The effect of α_c is presented in Section 4.1. If necessary, the Fourier image F_{xy} can be blurred before constructing a false colour image. This can be useful in high noise images.

3.3. Polarisation-resolved STED microscopy (pSTED)

Since polarisation is important to both excitation and emission of a fluorophore, it stands to reason that stimulated emission should also be polarisation dependent. In fact, that is what the calculation in Dyba et al.'s calculation of STED resolution is based on [17, 29]. Moreover, excitation and stimulated emission are described by the same quantum mechanical process [30].

Would it then be possible to adapt the principle of conventional STED microscopy to increase the polarisation resolution of a microscope, instead of its spatial resolution? In this section, I will introduce

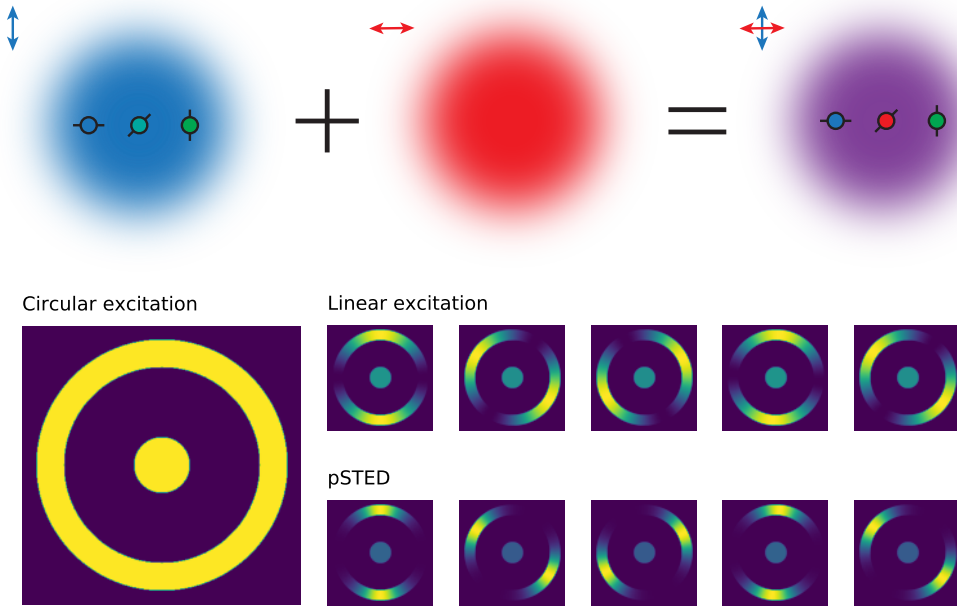


Figure 3.4: **Top:** Illustration of the working principle of pSTED. The arrows outside indicate the polarisation of the laser light. The circles represent fluorophores with their transition dipole moment indicated by a line. The orthogonal polarisation of the depletion beam suppresses fluorescence of the fluorophore oriented at 45°. **Bottom:** A simulation of pSTED compared to other excitation schemes on a sample consisting of a non-polarised disk and a radially polarised ring.

a definition of polarisation resolution, a mathematical description of how this might be improved using pSTED, and how we adapted the microscope setup in order to achieve that.

The general idea is that one can define a vectorial PSF (although a better term is photon fluence) that takes light polarisation into account. In a conventional polarisation microscopy setup, the probability of excitation of a fluorophore satisfies is proportional to $\cos^2 \Delta$, where Δ is the difference between the excitation polarisation and the transition dipole moment. This results in a FWHM resolution for conventional polarisation microscopy of

$$d_\theta = 90^\circ. \quad (3.13)$$

By illuminating the sample with a depletion beam that is orthogonally polarised to the excitation laser, we can suppress fluorescence of fluorophores on the edge of this PSF, just like in conventional STED. This is illustrated in Figure 3.4.

Derivation of the pSTED PSF. What follows is strongly inspired by Dyba et al. [29]. Let $\mathbf{x} = (x, y, z)$ be the spatial coordinates, θ be an angle with the x -axis in the xy plane (ranging from 0 to 2π) and ϕ be an angle with the z -axis in the xz plane (ranging from $-\pi$ to $+\pi$). We can also introduce a generalised coordinate $\mathbf{y} = (\mathbf{x}, \theta, \phi)$, which will be useful later.

Let the fluorophore population be described by the density $\rho(\mathbf{y})$. This function is normalised such that its integral is equal to the number of fluorophores. For example, a single fluorophore at the origin, pointing in the x direction with no out-of-plane tilt would be described by the Kronecker delta distribution $\rho_0 = \delta(\mathbf{y})$, which is defined as follows:

$$\delta(\mathbf{y}) = 0 \quad \text{if } y \neq 0, \quad (3.14)$$

$$\int f(\mathbf{y})\delta(\mathbf{y} - \mathbf{y}_0) d\mathbf{y} = f(\mathbf{y}_0). \quad (3.15)$$

The excitation beam is described by the electric field amplitude \mathbf{E}_{ex} , polarised along θ_{ex} , and analogous for the depletion beam. Like Equation 2.1, the emission intensity measured when the laser is focused on \mathbf{x} and polarised along θ, ϕ is now some sort of a convolution integral, where we also have to integrate

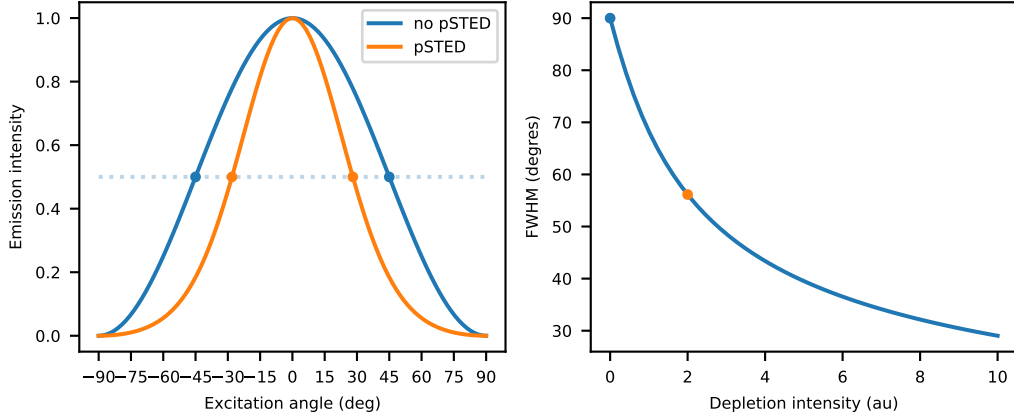


Figure 3.5: **Left:** Narrowing of the fluorophore response as a result of a depletion field (of intensity $I_d = 2$, as compared to the right pane). **Right:** The FWHM angular resolution d_θ as a function of depletion intensity.

over the angles θ and ϕ like

$$\begin{aligned} I_{em} &= A \int \sigma_{ex} |\hat{\mathbf{n}}_{\theta'\phi'} \cdot \mathbf{E}_{ex}(\mathbf{x} - \mathbf{x}')|^2 \rho(\mathbf{x}', \theta', \phi') d\mathbf{y}' \\ &= \int \sigma_{ex} I_{ex}(\mathbf{x}' - \mathbf{x}) |\hat{\mathbf{n}}_{\theta'\phi'} \cdot \hat{\mathbf{n}}_{\theta\phi}|^2 \rho(\mathbf{x}', \theta', \phi') d\mathbf{y}' \end{aligned} \quad (3.16)$$

where $\hat{\mathbf{n}}_{\theta\phi}$ is a unit vector pointing in the direction of (θ, ϕ) and $A = \epsilon_0 c / 2$. The dot product can be expressed as

$$|\hat{\mathbf{n}}_{\theta'\phi'} \cdot \hat{\mathbf{n}}_{\theta\phi}|^2 = \cos^2 \theta \cos^2 \phi, \quad (3.17)$$

so we can write that equation as a convolution product like

$$I_{em} = (\rho * h_{ex})(\mathbf{y}), \quad \text{where} \quad (3.18)$$

$$h_{ex}(\mathbf{y}) = \sigma_{ex} I_{ex}(\mathbf{x}) \cos^2(\theta) \cos^2(\phi). \quad (3.19)$$

If we have a constant laser intensity I_{ex} that is polarised along θ (without any out-of plane polarisation), this would reduce to

$$I_{em} = \sigma_{ex} I_{ex} \cos^2 \theta_{ex} \quad (3.20)$$

for the distribution ρ_0 . I_{em} is maximal when the excitation polarisation is in the x direction, as expected.

Now, we need to include the effect of the polarised depletion field, which amounts to adding an exponential factor under the integral

$$I_{em} = A \int \sigma_{ex} |\hat{\mathbf{n}}_{\theta'\phi'} \cdot \mathbf{E}_{ex}(\mathbf{x} - \mathbf{x}')|^2 \exp\left(-\sigma_d |\hat{\mathbf{n}}_{\theta'\phi'} \cdot \mathbf{E}_d(\mathbf{x} - \mathbf{x}')|^2\right) \rho(\mathbf{x}', \theta', \phi') d\mathbf{y}'. \quad (3.21)$$

In essence, we should then multiply the kernel h_{ex} with the function η

$$h_{pSTED}(\mathbf{y}) = h_{ex}(\mathbf{y}) \eta(\mathbf{y}) = \sigma_{ex} I_{ex}(\mathbf{x}) \cos^2(\theta) \exp(-\sigma_d I(\mathbf{x}) \sin^2 \theta), \quad (3.22)$$

which assumes both electric fields are orthogonally polarised and confined to the xy plane.

This model can easily be extended to account for depolarising effects such as rotational diffusion, energy transfer, et cetera. However, that is not necessary at this point. Instead, we would like to know the resolution improvement this gives us. With a little algebra, it can be shown that the the FWHM resolution satisfies

$$d_\theta(I_d) = 2 \arccos \sqrt{\frac{\mathcal{W}\left(\frac{\sigma_d I_d e^{\sigma_d I_d}}{2}\right)}{\sigma_d I_d}}, \quad (3.23)$$

where \mathcal{W} is the Lambert W-function. It is the inverse of the function $f(x) = xe^x$. As expected, $d_\theta(0) = 90^\circ$. $d_\theta(0)$ is plotted in Figure 3.5.

Implementation of pSTED. The system was not set up for tuning the depletion polarisation. Instead, the STED polarisation is always circular, and this is ensured by a set of two fixed waveplates: a QWP and a HWP (refer to Figure 3.1 and the description of the STED module in that section).

To control the polarisation of the depletion beam, I first had to linearise the polarisation by compensating for the QWP in the beam path. That can be done by placing a QWP in the pSTED module in Figure 3.1. This works because

$$S_{\lambda/4}(\phi)S_{\lambda/2}(0)S_{\lambda/4}(-\phi) = R(2\phi). \quad (3.24)$$

When the quarter-wave plates are aligned like that, this system simply rotates the polarisation by a fixed angle. Then, adding a HWP before this setup suffices to get full control over the polarisation angle of the depletion beam.

3.4. Samples

During the project, samples were very generously provided by research groups led by Pontus Nordenfelt and Vinay Swaminathan (Division of Infection Medicine, Faculty of Medicine, Lund University).

Results of the cell sample shown in the experimental section contain a human cell line infected with bacteria of the Yersinia genus. Stainings present are: DAPI (nucleus), GFP (bacteria) and SiR-actin. SiR-actin is an organic molecule (silicon-rhodamine) rigidly linked to an actin monomer. This dye is perfect for our setup, as SiR can be excited at 664 nm and has an sufficient absorption cross-section at 775 nm to perform STED. In addition, the fact that it is rigidly bound to the actin cytoskeleton means the light it emits is strongly polarised and reports on the the actin filament orientation.

I also used two control samples for calibration measurements. The first is a sample of small ([How small?](#)) reflective gold colloids, which were used to image the laser point spread functions. The second contains larger Tetraspec fluorescent beads (Invitrogen).

4

Results

4.1. Demonstration of conventional polarisation microscopy

Even though we can't use polarisation on the detection side yet, we can already make polarisation images by varying the angle of excitation polarisation. As a proof of concept, I imaged the sample described in Section 3.4, stepping the excitation light from 0° to 170° in steps of 10° . Applying the algorithm detailed in Section 3.2 to three different ROIs resulted in Figure 4.1. As expected, vertically oriented fibres are excited by horizontal polarisation [31].

I also included power law scaling of the saturation (degree of polarisation) and value (total brightness) in the visualisation algorithm. These serve to adjust the brightness and contrast of the figure, as shown in Figure 4.2.

To do:

- I could plot some histograms and stuff, of the polarisation distribution, but I guess that only really makes sense if I can actually make a substantial comment about it.
- sSTED + polarisation

4.2. Polarisation-resolved STED microscopy

In this section, I will detail how we implemented the pSTED scheme detailed in Section 3.3 and how we verified that it is working as predicted (rephrase if conclusion is that it doesn't work ye). The first step is to manipulate the polarisation of the depletion beam. Then I can do experiments on unpolarised and polarised controls (beads and Yersinia samples).

To get control of the light polarisation, the first step was to mount two new waveplates in the beam path. They were mounted after the SLM. A HWP was mounted inside a rotational stage and a QWP went in a cage system attached to the rotational stage, such that it is always aligned with the HWP, but that its rotational angle is fixed. The first step was to find the angle of the QWP that maximised the linearity of the light polarisation at the sample. This was simply done by placing a polariser and a power meter at the sample and rotating them to characterise the polarisation of the depletion beam. I did this

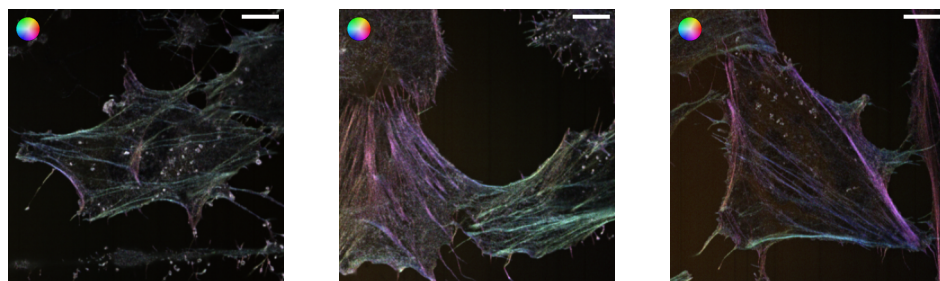


Figure 4.1: Polarisation microscopy images of three different cells. The colour wheel indicates the direction of polarised light corresponding to a certain colour. Scale bars $10\mu\text{m}$. (Get a camera view of with GFP and DAPI signals, see 21-02-05)

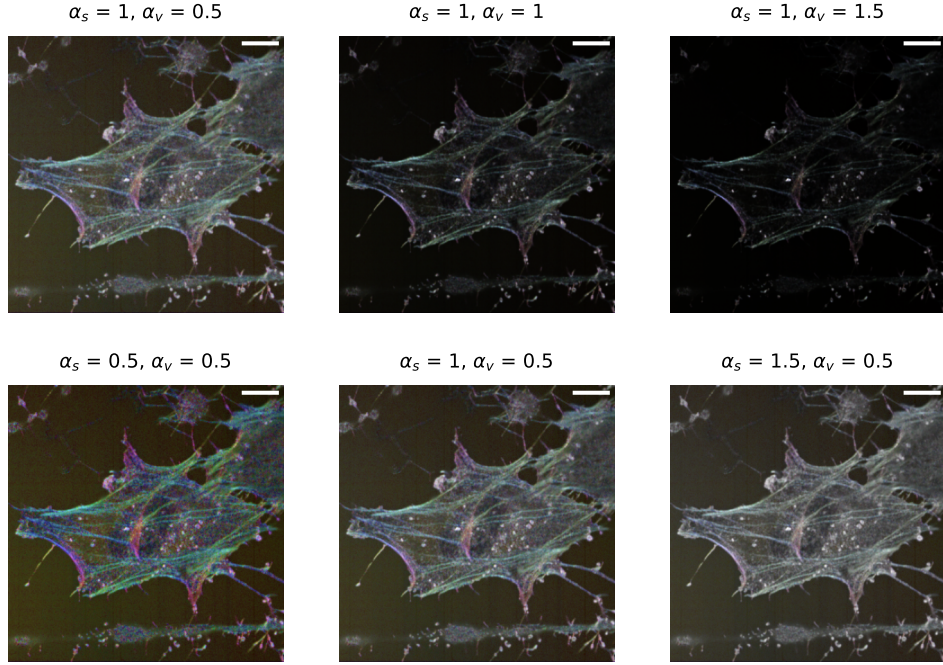


Figure 4.2: The effect of the exponents α_s (tuning saturation) and α_v (scaling brightness) on an image.

a couple of times, from which we concluded that the optimal angle for the QWP was 15° . Next, I had to find the angle of the HWP at which the depletion beam is vertically polarised. In that position, the depletion beam has a polarisation parallel to the excitation lasers (at 0°). This turned out to be 38.4° . See Figure D.6. At a linearity of $I_{max}/I_{min} = 5.47$ (corresponding to an ellipticity $\chi = 10.3^\circ$) (depends on definition of χ again), the polarisation of the linearised pSTED beam is comparable in quality to the 640 laser.

Now that we have control over the beam polarisation, we can check how the added waveplates influence the PSF. In Figure D.7, the PSF is shown for different polarisation directions. There are a number of conclusions we can draw from this data. Firstly, the PSF is not radially symmetric any longer, even though the SLM was set to Gaussian mode. In particular, the ellipse orientation is parallel to the light polarisation, so we see the PSF rotating as we change the polarisation. This can be explained by the fact that a lens interacts differently with light polarised along different directions [32]. This is the reason one should only use linearly polarised excitation light when performing polarisation microscopy.

Other effects of the polarisation include the following: the intensity of the depletion beam varies as a function of the polarisation angle. This is probably due to linear dichroism present in the optical elements between the waveplates and the sample. That is to be expected, but should be accounted during either image acquisition or analysis. Furthermore, the eccentricity of the ellipse has a slight dependency on the polarisation angle, and the maximum of the PSF moves a little: up to (?) nm from its mean position. Fortunately this is a quite a bit below the diffraction limit for 775 nm light, i.e. around 400 nm. (Plot this data!)

(NOTE THAT WE HAVE TO ROTATE THE HWP BACKWARDS!!!!!!)

Finally, we can perform pSTED on some control samples. I used two different ones: a sample of non-polarised beads and the cell sample shown earlier. Isotropic beads are useful, since we can determine the polarisation of emitted light by selectively activating fluorophores of a particular orientation with the polarisation of the excitation light. This process is called photoselection. When these beads are excited with circularly polarised light, fluorophores of all orientations should be activated equally, and the polarisation of the depletion beam should not matter. In the case of linearly polarised excitation light, on the other hand, depletion should be more efficient when its polarisation is aligned with the excitation beam. This can be verified by increasing the depletion power: when the beams are aligned, then the remaining fluorescence signal should drop faster than when they are not, as predicted by Equation 3.21. Figure 4.3 shows that this is indeed the case. While there is some variation in the depletion rate under circular excitation, it can not be explained by the theory and seems random, unlike the case of linear excitation. There, depletion goes fastest when the beams are aligned, slower when there is a 45° angle

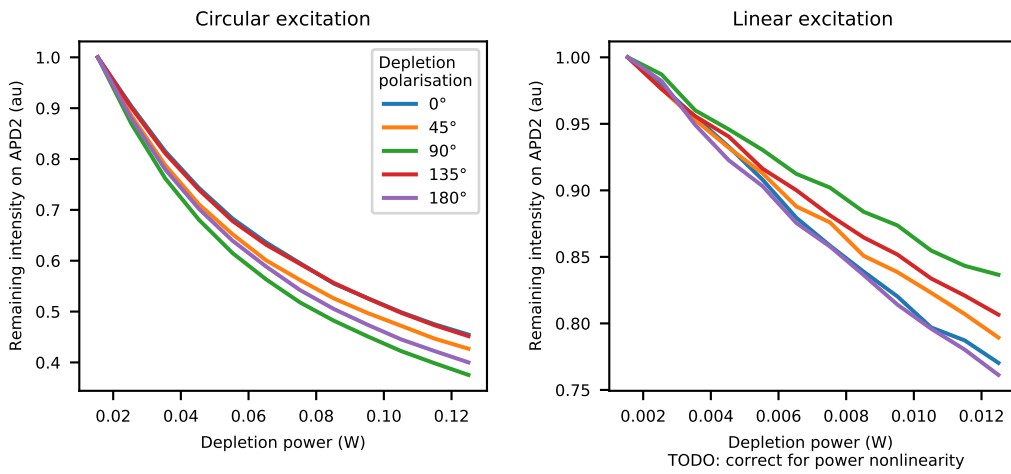


Figure 4.3: Dependency of surviving fluorescence on intensity and polarisation of depletion beam. **Left:** circular excitation. **Right:** linear excitation at 0° (vertical). (Planning to do a number of repeats to get rid of noise in this figure.)

between them, and slowest when they are orthogonal. If the depletion beam was more linearly polarised (i.e. had a lower χ), then this effect would be even more pronounced.

(pSTED results in cells. Mention spacer channels. Mention that pSTED intensity shouldn't be too high, otherwise you'll never see anything.)

5

Outlook

- Conventional polarisation microscopy
 - Figure out detection waveplates, otherwise you can't use polarisation in the detection pathway
 - I've made some measurements of polarisation sensitivities etc. We need to set up an analysis pipeline that makes use of them to correct systematic data errors before we can make quantitative statements about sample polarisation. Then we should really compare it to data from another lab and see if it matches.
 - better pol sensitivity measurement with an artificial molecule
 - As part of that, tune the 640 and 775 waveplates to increase linearity to match the 561 laser.
 - Improve the excitation waveplate calibration.
- Keep developing pSTED
- Other fancy polarisation stuff: FLIM + pol, FRET measurements, ...
- To do actual biological research, conventional pol microscopy is definitely the way to go. sSTED is easier than pSTED (for now).

Bibliography

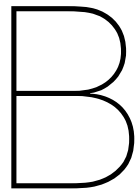
- [1] J. van Zuylen. The microscopes of Antoni van Leeuwenhoek. *Journal of Microscopy*, 121(3):309–328, 1981. DOI: [10.1111/j.1365-2818.1981.tb01227.x](https://doi.org/10.1111/j.1365-2818.1981.tb01227.x).
- [2] Ernst Abbe. Beiträge zur Theorie des Mikroskops und der mikroskopischen Wahrnehmung. *Archiv für mikroskopische Anatomie*, 9(1):413–468, 1873.
- [3] David J. Smith. Ultimate resolution in the electron microscope? *Materials Today*, 11(SUPPL.):30–38, 2008. DOI: [10.1016/S1369-7021\(09\)70005-7](https://doi.org/10.1016/S1369-7021(09)70005-7).
- [4] John SH Danial, Yasmine Aguib, and Magdi H Yacoub. Advanced fluorescence microscopy techniques for the life sciences. *Global Cardiology Science and Practice*, 2016(2), 2016. DOI: [10.21542/gcsp.2016.16](https://doi.org/10.21542/gcsp.2016.16).
- [5] Jin Zhang, Robert E. Campbell, Alice Y. Ting, and Roger Y. Tsien. Creating new fluorescent probes for cell biology. *Nature Reviews Molecular Cell Biology*, 3(12):906–918, 2002. DOI: [10.1038/nrm976](https://doi.org/10.1038/nrm976).
- [6] Ute Resch-Genger, Markus Grabolle, Sara Cavaliere-Jaricot, Roland Nitschke, and Thomas Nann. Quantum dots versus organic dyes as fluorescent labels. *Nature Methods*, 5(9):763–775, 2008. DOI: [10.1038/nmeth.1248](https://doi.org/10.1038/nmeth.1248).
- [7] Nathan C. Shaner, Paul A. Steinbach, and Roger Y. Tsien. A guide to choosing fluorescent proteins. *Nature Methods*, 2(12):905–909, 2005. DOI: [10.1038/nmeth819](https://doi.org/10.1038/nmeth819).
- [8] Mikhail E. Matlashov, Daria M. Shcherbakova, Jonatan Alvelid, Mikhail Baloban, Francesca Pennacchietti, Anton A. Shemetov, Ilaria Testa, and Vladislav V. Verkhusha. A set of monomeric near-infrared fluorescent proteins for multicolor imaging across scales. *Nature Communications*, 11(1):1–12, 2020. DOI: [10.1038/s41467-019-13897-6](https://doi.org/10.1038/s41467-019-13897-6).
- [9] C. W. McCutchen. Superresolution in microscopy and the Abbe resolution limit. *Journal of the Optical Society of America*, 57(10):1190–1192, 1967. DOI: [10.1364/JOSA.57.001190](https://doi.org/10.1364/JOSA.57.001190).
- [10] Michael J. Rust, Mark Bates, and Xiaowei Zhuang. Sub-diffraction-limit imaging by stochastic optical reconstruction microscopy (STORM). *Nature Methods*, 3(10):793–795, 2006. DOI: [10.1038/nmeth929](https://doi.org/10.1038/nmeth929).
- [11] Eric Betzig, George H. Patterson, Rachid Sougrat, O. Wolf Lindwasser, Scott Olenych, Juan S. Bonifacino, Michael W. Davidson, Jennifer Lippincott-Schwartz, and Harald F. Hess. Imaging intracellular fluorescent proteins at nanometer resolution. *Science*, 313(5793):1642–1645, 2006. DOI: [10.1126/science.1127344](https://doi.org/10.1126/science.1127344).
- [12] Thomas A. Klar, Stefan Jakobs, Marcus Dyba, Alexander Egner, and Stefan W. Hell. Fluorescence microscopy with diffraction resolution barrier broken by stimulated emission. *Proceedings of the National Academy of Sciences of the United States of America*, 97(15):8206–8210, 2000. DOI: [10.1073/pnas.97.15.8206](https://doi.org/10.1073/pnas.97.15.8206).
- [13] Jonas Fölling, Mariano Bossi, Hannes Bock, Rebecca Medda, Christian A. Wurm, Birka Hein, Stefan Jakobs, Christian Eggeling, and Stefan W. Hell. Fluorescence nanoscopy by ground-state depletion and single-molecule return. *Nature Methods*, 5(11):943–945, 2008. DOI: [10.1038/nmeth.1257](https://doi.org/10.1038/nmeth.1257).
- [14] Michael Hofmann, Christian Eggeling, Stefan Jakobs, and Stefan W. Hell. Breaking the diffraction barrier in fluorescence microscopy at low light intensities by using reversibly photoswitchable proteins. *Proceedings of the National Academy of Sciences of the United States of America*, 102(49):17565–17569, 2005. DOI: [10.1073/pnas.0506010102](https://doi.org/10.1073/pnas.0506010102).
- [15] Dominik Wildanger, Brian R. Patton, Heiko Schill, Luca Marseglia, J. P. Hadden, Sebastian Knauer, Andreas Schönle, John G. Rarity, Jeremy L. O'Brien, Stefan W. Hell, and Jason M. Smith. Solid immersion facilitates fluorescence microscopy with nanometer resolution and sub-Ångström emitter localization. *Advanced Materials*, 24(44):309–313, 2012. DOI: [10.1002/adma.201203033](https://doi.org/10.1002/adma.201203033).

- [16] Albert Einstein. Zur Quantentheorie der Strahlung. *Zeitschrift für Physik*, 35(5):317–322, 1926. DOI: 10.1007/BF01380146.
- [17] Benjamin Harke, Jan Keller, Chaitanya K. Ullal, Volker Westphal, Andreas Schönle, and Stefan W. Hell. Resolution scaling in STED microscopy. *Optics Express*, 16(6):4154, 2008. DOI: 10.1364/oe.16.004154.
- [18] Tobias Müller, Christian Schumann, and Annette Kraegeloh. STED microscopy and its applications: New insights into cellular processes on the nanoscale. *ChemPhysChem*, 13(8):1986–2000, 2012. DOI: 10.1002/cphc.201100986.
- [19] Eitan Lerner, Anders Barth, Jelle Hendrix, Benjamin Ambrose, Victoria Birkedal, Scott C Blanchard, Richard Börner, Hoi Sung Chung, Thorben Cordes, Timothy D. Craggs, Ashok A. Deniz, Jiajia Diao, Jingyi Fei, Ruben L. Gonzalez, Irina V. Gopich, Taekjip Ha, Christian A. Hanke, Gilad Haran, Nikos S. Hatzakis, Sungchul Hohng, Seok Cheol Hong, Thorsten Hugel, Antonino Ingargiola, Chirlmin Joo, Achillefs N. Kapanidis, Harold D. Kim, Ted Laurence, Nam Ki Lee, Tae Hee Lee, Edward A. Lemke, Emmanuel Margeat, Jens Michaelis, Xavier Michalet, Sua Myong, Daniel Nettels, Thomas Otavio Peulen, Evelyn Ploetz, Yair Razvag, Nicole C. Robb, Benjamin Schuler, Hamid Soleimaninejad, Chun Tang, Reza Vafabakhsh, Don C. Lamb, Claus A.M. Seidel, Shimon Weiss, and Olga Boudker. FRET-based dynamic structural biology: Challenges, perspectives and an appeal for open-science practices, 2021. ISSN 2050084X.
- [20] Adam S. Backer, Andreas S. Biebricher, Graeme A. King, Gijs J.L. Wuite, Iddo Heller, and Erwin J.G. Peterman. Single-molecule polarization microscopy of DNA intercalators sheds light on the structure of S-DNA. *Science Advances*, 5(3), 2019. DOI: 10.1126/sciadv.aav1083.
- [21] Pontus Nordenfelt, Travis I. Moore, Shalin B. Mehta, Joseph Mathew Kalappurakkal, Vinay Swaminathan, Nobuyasu Koga, Talley J. Lambert, David Baker, Jennifer C. Waters, Rudolf Oldenbourg, Tomomi Tani, Satyajit Mayor, Clare M. Waterman, and Timothy A. Springer. Direction of actin flow dictates integrin LFA-1 orientation during leukocyte migration. *Nature Communications*, 8(1), 2017. DOI: 10.1038/s41467-017-01848-y.
- [22] Vinay Swaminathan, Joseph Mathew Kalappurakkal, Shalin B. Mehta, Pontus Nordenfelt, Travis I. Moore, Nobuyasu Koga, David A. Baker, Rudolf Oldenbourg, Tomomi Tani, Satyajit Mayor, Timothy A. Springer, and Clare M. Waterman. Actin retrograde flow actively aligns and orients ligand-engaged integrins in focal adhesions. *Proceedings of the National Academy of Sciences of the United States of America*, 114(40):10648–10653, 2017. DOI: 10.1073/pnas.1701136114.
- [23] Sophie Brasselet, Patrick Ferrand, Alla Kress, Xiao Wang, Hubert Ranchon, and Alicja Gasecka. *Imaging Molecular Order in Cell Membranes by Polarization-Resolved Fluorescence Microscopy*, pages 311–337. Springer Berlin Heidelberg, Berlin, Heidelberg, 2013. ISBN 978-3-642-33128-2. DOI: 10.1007/4243_2012_51.
- [24] D. Goldstein. *Polarised light*. Taylor and Francis Group, 3 edition, 2011. ISBN 9781439830413.
- [25] Edward Collett. *Field guide to polarization*. The Society of Photo-Optical Instrumentation Engineers, 2005. ISBN 0819458686.
- [26] Joseph R. Lakowicz. *Principles of fluorescence spectroscopy*. Springer, third edition edition, 2006.
- [27] Rafael Camacho, Daniela Täuber, and Ivan G. Scheblykin. Fluorescence Anisotropy Reloaded—Emerging Polarization Microscopy Methods for Assessing Chromophores’ Organization and Excitation Energy Transfer in Single Molecules, Particles, Films, and Beyond. *Advanced Materials*, 1805671:1–30, 2019. DOI: 10.1002/adma.201805671.
- [28] Georgios D. Evangelidis and Emmanouil Z. Psarakis. Parametric image alignment using enhanced correlation coefficient maximization. *IEEE Transactions on Pattern Analysis and Machine Intelligence*, 30(10):1858–1865, 2008. DOI: 10.1109/TPAMI.2008.113.
- [29] M. Dyba, J. Keller, and S. W. Hell. Phase filter enhanced STED-4Pi fluorescence microscopy: Theory and experiment. *New Journal of Physics*, 7, 2005. DOI: 10.1088/1367-2630/7/1/134.
- [30] Christopher J. Foot. *Atomic Physics*. Oxford University Press, 2005.

- [31] Felix Spira, Sara Cuylen-Haering, Shalin Mehta, Matthias Samwer, Anne Reversat, Amitabh Verma, Rudolf Oldenbourg, Michael Sixt, and Daniel W Gerlich. Cytokinesis in vertebrate cells initiates by contraction of an equatorial actomyosin network composed of randomly oriented filaments. *eLife*, 6: 1–24, 2017. DOI: 10.7554/eLife.30867.
- [32] Alexander Egner, Claudia Geisler, and René Siegmund. STED Nanoscopy. In *Nanoscale Photonic Imaging*, volume 134, chapter 1, pages 3–34. Springer, 2020. ISBN 9783030344122. DOI: 10.1007/978-3-030-34413-9_14.
- [33] Arbetsmiljöverket. Artificiell optisk strålning, arbetsmiljöverkets föreskrifter om artificiell optisk strålning och allmänna råd om tillämpningen av föreskrifterna. <https://www.av.se/globalassets/filer/publikationer/foreskrifter/artificiell-optisk-stralning-foreskrifter-afs2009-7.pdf>, 2019. Accessed: 2021-03-15.

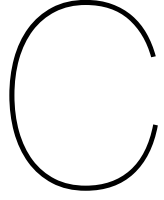
A

Acknowledgements



Code and data availability

I've spent quite a bit of effort ensuring this entire thesis easily reproducible from the raw data. To that end, the source code and data necessary to produce this file and the figures in it are published on GitHub, at <https://github.com/wduverger/msc-thesis>. If you experience any trouble getting the code to run, have any questions regarding this thesis or just want to chat about polarisation microscopy in general, please reach out! I am always happy to help.



A note on laser safety

The 775 nm line is a class 4 laser source. Under normal operation, the user is protected from it. However, when calibrating the STED beam or placing new components in the beam path, it is theoretically possible for the collimated laser beam to be reflected into the user's eyes. A high-powered laser beam can do permanent damage to the skin and retina, so we have to make sure we stay below the limits imposed by the Work Environment Agency's (Arbetsmiljöverkets) limits [33]. These regulations set forth three main conditions to calculate the Maximum Permissible Exposure (MPE) of a pulsed laser, see table 2.6 of the regulations. Important values and formulas about our setup, as well as the limits provided by the Work Environment Agency are provided in Table C.1 and in the text below.

Table C.1: Operating characteristics of the 775 laser line and relevant safety parameters.

Quantity	Symbol	Value
Laser operating characteristics		
Beam radius	r	0.5 mm
Pulse width (FWHM)	τ	1.3 ns
Pulse repetition frequency	f	40 MHz
Pulse energy	E_{pulse}	31 nJ
Average power	P_{avg}	1.25 W
Safety parameters		
Thermal correction time	T_{min}	18 μ s
C_a	C_a	1.41
C_c	C_c	1
C_e	C_e	1

Rule 1: The dose of a single pulse must not exceed the single-pulse MPE. The pulse dose H_{pulse} of the 775 nm laser at full power is

$$H_{pulse} = \frac{E_{pulse}}{2\pi r^2} \approx 39 \text{ mJ/m}^2, \quad (\text{C.1})$$

whereas the MPE equals

$$H_{pulse}^{MPE} = 5 \times 10^{-3} C_a C_e = 7.1 \text{ mJ/m}^2. \quad (\text{C.2})$$

This formula is found in table 2.2 of the regulations.

Rule 2: The dose of a single pulse may not exceed the thermally-corrected MPE. This weighs the pulse MPE with the amount of pulses in an interval T_{min} . The number of pulses in such an interval is $n = f \cdot T_{min}$, so

$$H_{thermal}^{MPE} = n^{-1/4} H_{pulse}^{MPE} = 1.3 \text{ mJ/m}^2. \quad (\text{C.3})$$

Rule 2 is therefore more strict than the rule 1. For safe operation, the laser must be ran at a power below 3.3% ($= H_{thermal}^{MPE}/H_{pulse}$).

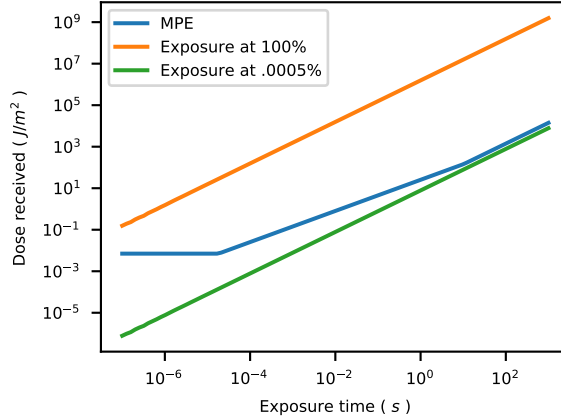


Figure C.1: Maximum permissible and actual exposure to the collimated STED beam as a function of exposure time.

Rule 3: The cumulative dose for a group of pulses in an interval of time t must not exceed the MPE for a single pulse of that time. Taking the necessary values from tables 2.2 and 2.3, the cumulative MPE is defined as

$$H_{tot}^{MPE}(t) = \begin{cases} 5 \times 10^{-3} C_a C_e & t < 18 \mu\text{s}, \\ 18t^{0.75} C_a C_e & 18 \mu\text{s} < t < 10 \text{ s}, \\ 10t C_a C_c & t > 10 \text{ s}. \end{cases} \quad (\text{C.4})$$

The actual dose, on the other hand, is

$$H_{tot}(t) = \lfloor ft \rfloor H_{pulse}, \quad (\text{C.5})$$

where $\lfloor \cdot \rfloor$ is the flooring function. This function is plotted in Figure C.1, from which it can be seen that the laser is only safe to use at 0.0005% capacity. Since the minimum laser power offered by the software is .05% (check if this makes sense with Jason's laser power data), OD2 goggles should be worn to guarantee safe operation of the 775 nm laser.

(I did some calculations on laser tolerance when we were ordering the pSTED optics. Would it be worth it to put those in?)

D

Supplemental figures

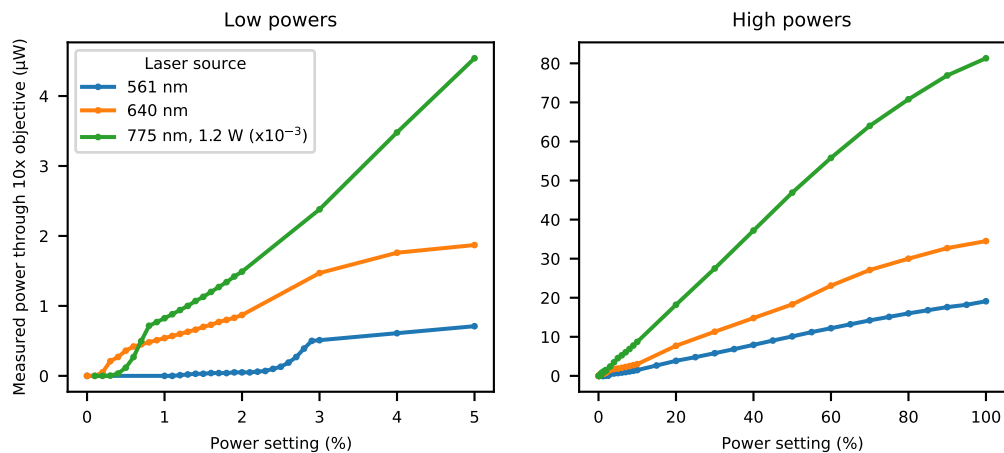


Figure D.1: The power of each of the three lasers as measured through a 10x objective. Notice the non-linearity at low power settings. The 775 nm data was scaled down by three orders of magnitude. [\(reference to figure\)](#)

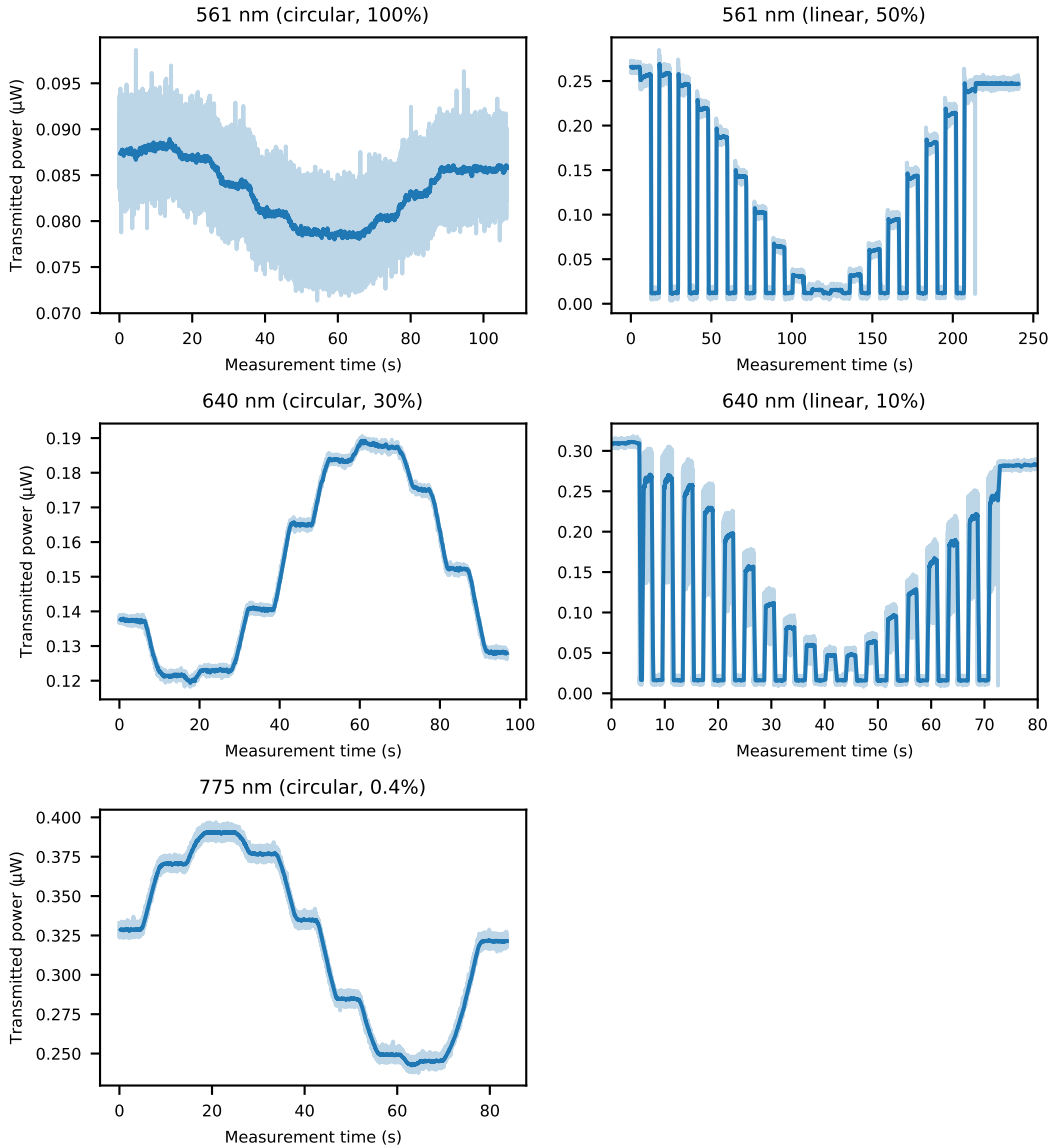


Figure D.2: Polarisation characterisation of the different lasers. To characterise circular polarisation, a polariser was placed in the sample and scanned from 0° to 180° in steps of 20° (notice that I forgot to sample 260° in the 775 nm data). Linear polarisation was characterised by fixing the polariser in place at 0° and scanning the laser itself from 0° to 180° in steps of 10° . Dark blue: average over 200 samples, light blue: raw data.

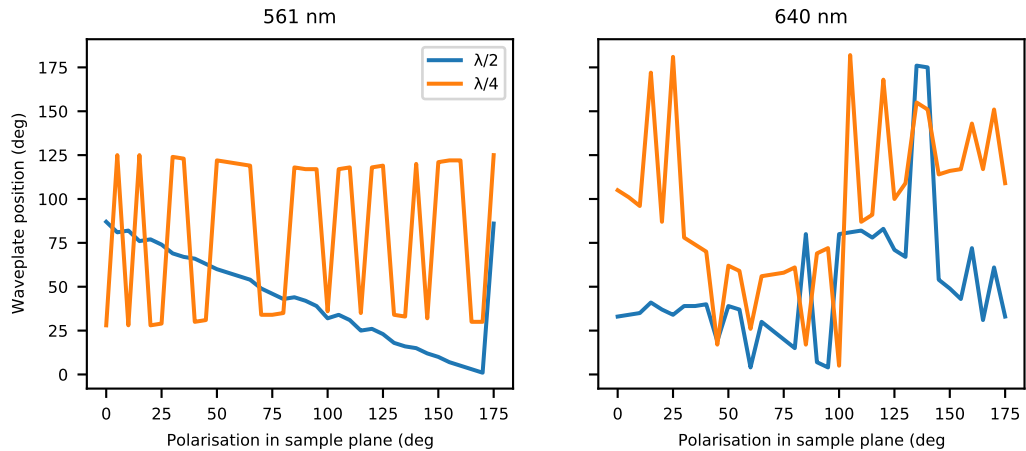


Figure D.3: Calibrations of the excitation waveplates, as supplied by the microscope manufacturer.

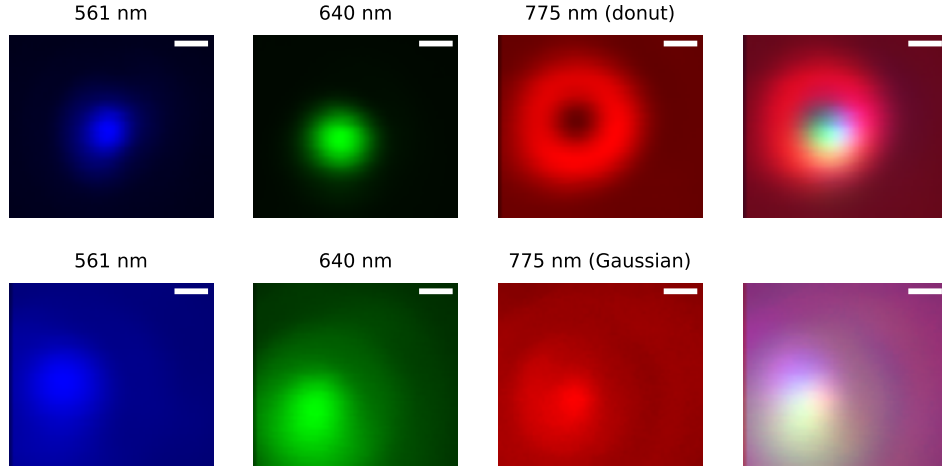


Figure D.4: Point spread functions of the different lasers at different SLM configurations, by measuring the reflection from 100 nm wide gold beads. Scale bars 200 nm. [\(show better data from 26 march\)](#)

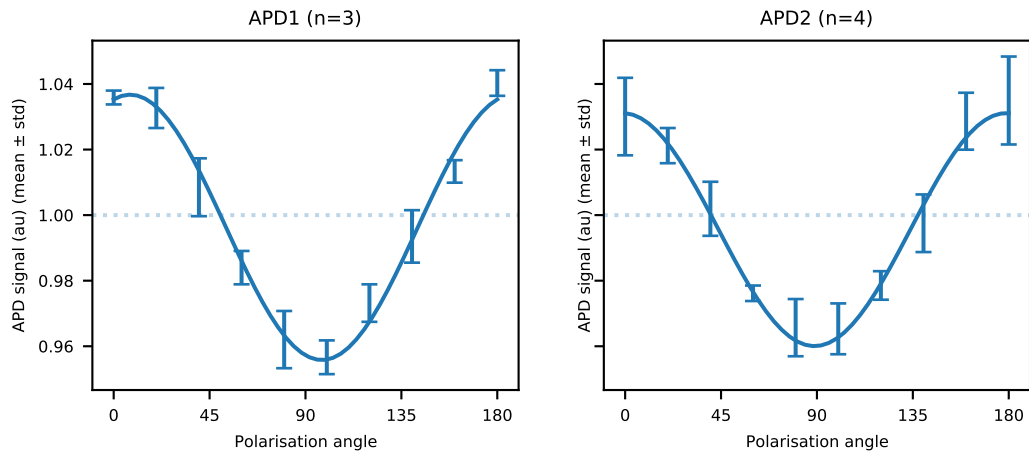


Figure D.5: Dependence of the signal from APD1 on the angle of polarisation of incoming light.

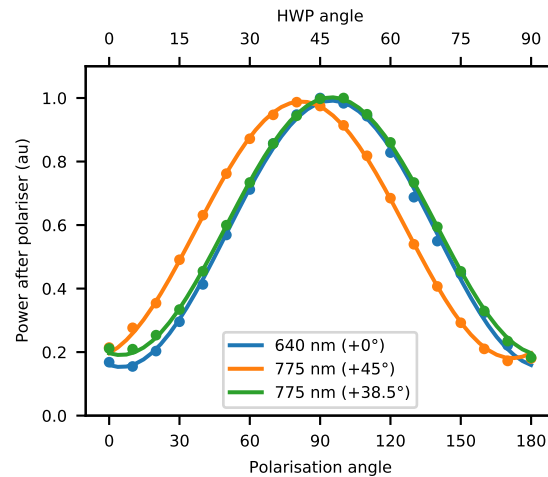


Figure D.6: The rotating HWP I put in the beamline controls the depletion beam polarisation. With an offset of 38.4°, the depletion beam is parallel to the 640 laser (set to vertical linear polarisation).

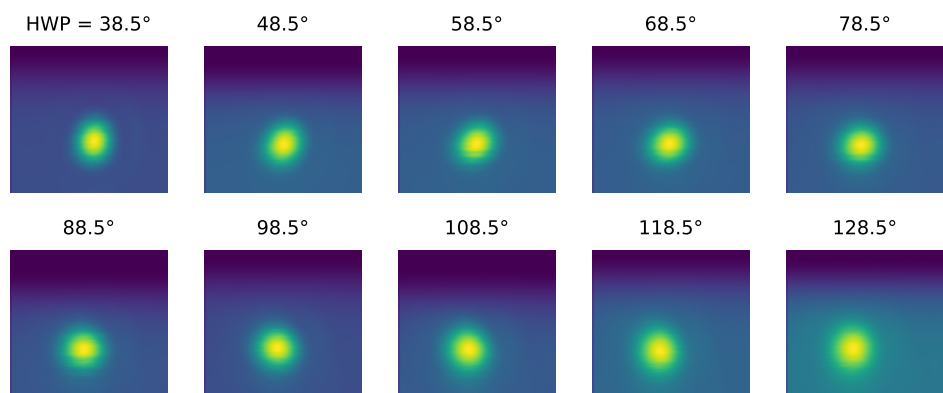


Figure D.7: Depletion PSF as a function of beam polarisation. (Why the change in background levels?)